Available online at www.sciencedirect.com
SCIENCE DIRECT®
Journal of Solid State Chemistry 177 (2004) 3896–3902
JOURNAL OF SOLID STATE CHEMISTRY
www.elsevier.com/locate/jssc

Rare-earth-rich tellurides: Gd_4NiTe_2 and $Er_5M_2Te_2$ (M = Co, Ni)

Carmela Magliocchi, Fanqin Meng, Timothy Hughbanks*

Department of Chemistry, Texas A&M University, TAMU 3255, P.O. Box 30012, College Station, TX 77842-3012, USA

Received 16 April 2004; received in revised form 8 July 2004; accepted 12 July 2004
Available online 18 September 2004

Abstract

Three new rare earth metal-rich compounds, Gd_4NiTe_2, and $Er_5M_2Te_2$ (M = Ni, Co), were synthesized in direct reactions using R, R_3M, and R_2Te_3 (R = Gd, Er; M = Co, Ni) and single-crystal structures were determined. Gd_4NiTe_2 is orthorhombic and crystallizes in space group *Pnma* with four formula units per cell. Lattice parameters at 110(2) K are $a = 15.548(9)$, $b = 4.113(2)$, $c = 11.7521(15)$ Å. $Er_5Ni_2Te_2$ and $Er_5Co_2Te_2$ are isostructural and crystallize in the orthorhombic space group *Cmcm* with two formula units per cell. Lattice parameters at 110(2) K are $a = 3.934(1)$, $b = 14.811(4)$, $c = 14.709(4)$ Å, and $a = 3.898(1)$, $b = 14.920(3)$, $c = 14.889(3)$ Å, respectively. Metal–metal bonding correlations were analyzed using the empirical Pauling bond order concept.

Keywords: Crystal structure; Rare-earth telluride; Intermetallic Bonding; Chalcogenide

1. Introduction

Synthetic exploration of metal-rich chalcogenides guided by Brewer's Lewis-acid–base concept of polar intermetallic bonding has focused on the early transition metals, namely, Zr, Hf, Nb and Ta [1]. Brewer's viewpoint, in which electron donation from late-transition elements to early transition elements is seen as especially important, has been extended to ternary compounds of the electron-poor rare-earth metal systems and has led to the expectation and realization of many new compounds with novel compositions, structures, and properties. These include $Sc_5Ni_2Te_2$ [2], Dy_6MTe_2 (M = Fe, Co, Ni) [3], R_6CoTe_2 (R = Y, La) [3], Sc_6MTe_2 (M = Mn, Fe, Co, Ni) [4], which were synthesized and characterized. Our group has reported the synthesis of Zr_6MTe_2 (M = Mn, Fe, Co, Ni, Ru, Pt) and $Zr_6Fe_{1-x}Q_{2+x}$,(Q = Se, S) [5], Gd_6MTe_2 (M = Ni, Co) and Er_6RuTe_2 [6], Hf_5FeTe_3 and Hf_8FeTe_6 (M = Mn, Fe) [7], and $Er_7Ni_2Te_2$ [8].

New compounds Gd_4NiTe_2 and $Er_5M_2Te_2$ (M = Co, Ni) discussed in this paper are among the most metal-rich of the ternary rare-earth-metal chalcogenides. The principal structural feature in this class of compounds is the centered tricapped trigonal prism (TTP). These are condensed into infinite chains in a manner are similar to those found in Gd_3MnI_3 [9], Y_3MI_3 (M = Ru, Ir) [10], $Sc_5Ni_2Te_2$ [2], $Y_5Ni_2Te_2$ and (M = Fe, Co, Ni) [11]. This paper presents the synthesis and structural features of new compounds, $Er_5M_2Te_2$ (M = Co, Ni), isotypic with $Y_5Ni_2Te_2$, and Gd_4NiTe_2, a structure-type in a new class of metal-rich telluride compounds. Evident structural relationships between the title compounds and other intermetallic compounds are discussed with respect to the condensation of the metal–metal bonded framework.

2. Experimental

2.1. Techniques and materials

All materials were manipulated in a nitrogen atmosphere glovebox or vacuum line. Gd and Er foils (99.99 at%, Ames Laboratory), and Co, Ni (both 99.998%, Alfa Aesar), and Te (99.997%, Aldrich)

*Corresponding author. Fax: +1-979-847-8860.
E-mail address: trh@mail.chem.tamu.edu (T. Hughbanks).

0022-4596/$ - see front matter © 2004 Elsevier Inc. All rights reserved.
doi:10.1016/j.jssc.2004.07.019

powders (at%, metals basis) were used as purchased. Ames Laboratory carbon and oxygen analysis for the Gd and Er metals were <0.0002 and <0.0003 at%, respectively. R_2Te_3 compounds were made in stoichiometric reactions of the constituent elements in evacuated silica tubes at 750–850 °C, as described in the literature [12]. R_3M (M = Co, Ni) compounds were synthesized by arc melting cold-pressed pellets (crushed foils or chips) of R and M in 3:1 ratio. Nb tubes were used as the reaction containers to make the ternary compounds—stoichiometric proportions of reactants were loaded in Nb tubes that were welded under an argon atmosphere (150–250 torr). The Nb tubes were then sealed in an evacuated silica jacket and heated in an electric furnace.

2.2. Syntheses

Gd_4NiTe_2 was first discovered in an attempt to synthesize a Ni containing compound with the Gd_6MTe_2 structure [6]. Stoichiometric proportions of Gd, Gd_3Ni, and Gd_2Te_3 in the presence of few milligrams of $GdBr_3$ (added in an attempt to promote vapor phase transport) were loaded into a niobium tube and welded. In some instances, molybdenum foils were used to minimize tellurium attack on the Nb tube; for the same reason, reaction temperatures were ramped to 550 °C over 2 days, maintained there for 2 more days, then steadily raised to 1000 °C over 4 days. After 8 days at 1000 °C, the reaction was cooled to 500 °C over 4 days and then cooled to room temperature. The powder diffraction pattern revealed a mixture of Gd_4NiTe_2 as the major phase (yield: 80–90%); GdTe was the minor phase. Single-crystal diffraction (see below) determined the identity of Gd_4NiTe_2, and further reactions with the 4:1:2 stoichiometry were attempted. These yielded mostly the binary phase GdTe. Nb was not detected in EDS analyses of products, but tubes were not scraped after reaction either—in some cases the Nb tubes showed some embrittlement indicative of attack. Much better yields of Gd_4NiTe_2 were achieved by loading reactions with excess Gd. In all these cases, the temperature profile was not varied, and no $GdBr_3$ was included.

$Er_5Ni_2Te_2$ was first discovered as single crystals in a reaction intended to make $Er_7Ni_2Te_2$. Subsequent reactions were loaded to make $Er_5Ni_2Te_2$ by combining Er_3Ni, $NiTe_2$, and Er in a 1:1:2 mole ratio. As usual, Nb tubes were used as reaction containers that in turn were sealed in evacuated silica jackets. Since all the starting materials have low volatility, the reaction temperature was ramped directly up to 1000 °C over 24 h and maintained there for three weeks. The reaction was cooled radiatively afterwards. The Guinier powder diffraction pattern of the product indicated the desired ternary compound was made in ~85% yield and ErTe coexisted as a minor phase. $Er_5Co_2Te_2$ was synthesized analogously. Reactions run at 850 °C for a month yielded the title compounds with poor crystallinity. Guinier powder patterns of the lower-temperature products appear to be "clean", but the presence of other phases might not be detectable by due to their poor crystallinity.

2.3. X-ray crystallography

Single-crystal X-ray diffraction data were collected at 110(2) K using a Siemens (Bruker) diffractometer equipped with SMART CCD and a graphite monochromator using Mo$K\alpha$ radiation ($\lambda = 0.71073$ Å) with a LT-2 low-temperature apparatus. Data were measured using omega scans of 0.3° per frame for 40 s, such that a hemisphere was collected. The first 50 frames were used as check reflections at the end of the data collection. Cell parameters were retrieved using SMART software [13] and data reduction was performed using SAINT, which corrects for Lorentz polarization and decay [14]. SADABS was used to make absorption corrections [15]. The structures were then solved by direct methods using the SHELXS program and refined with the full-matrix least-squares program SHELXL and the remaining atomic positions were located from the electron density difference maps using the SHELXTL package [16]. All atoms were refined anisotropically.

The reaction loaded to make Gd_6NiTe_2 produced a good yield of reflective, dark, rod-like, single crystals, but which proved to be Gd_4NiTe_2. A suitable crystal with dimensions $0.003 \times 0.01 \times 0.17\,mm^3$ was coated with Apiezon®-T stopcock grease, subsequently mounted on the tip of a glass fiber, and immediately inserted into the low-temperature nitrogen stream of the diffractometer for data collection. A total of 4689 reflections ($4.34° < 2\theta < 55°$, $\pm h$, $\pm k$, $\pm l$) were collected and 1046 were unique. Initially, the refinement yielded systematically oblate displacement parameters for all atoms, illustrating an inadequate absorption correction. Therefore we performed an empirical absorption correction on the raw data using the empirical DIFABS program, which applies an empirical absorption correction based on direction cosines by fitting the observed data to calculated intensities. The data was then refined in SHELXL-97 and the displacement parameters were approximately spherical. A total of 44 variables were used in the refinements and data converged to $R_1 = 0.0568$, w$R_2 = 0.1327$ (all data).

A black rod-shaped single crystal of $Er_5Ni_2Te_2$ with dimensions of $0.18 \times 0.04 \times 0.01\,mm^3$ was picked from the reaction product, protected with a thin layer of Apiezon-T grease and mounted on the tip of a glass fiber. Data collection and structural refinements were carried out following the same procedure as for the

Table 1
Crystallographic data for metal-rich ternary tellurides

Chem. formula	Gd_4NiTe_2	$Er_5Ni_2Te_2$	$Er_5Co_2Te_2$
fw, g/mol	3771.64	1208.92	1209.36
Space group	*Pnma*	*Cmcm*	*Cmcm*
a (Å)	15.548(9)	3.9338(11)	3.8976(8)
b (Å)	4.113(2)	14.811(4)	14.920(3)
c (Å)	11.752(7)	14.709(4)	14.889(3)
V (Å^3)	751.6(7)	857.0(4)	865.8(3)
Z	4	2	2
T (K)	110(2)	110(2)	110(2)
λ (Mo*K*α)(Å)	0.71073	0.71073	0.71073
ρ_{calcd}(g/cm^3)	8.333	4.685	4.639
μ (mm^{-1})	44.755	29.628	29.069
R_1[a], ($I>2\sigma(I)$)	0.0568	0.0661	0.0979
wR^{2}[b]	0.1327	0.1574	0.1202

[a] $R_1 = \Sigma| |F_o|—|F_c| |/\Sigma|F_o|$.
[b] $wR_2 = [\Sigma[w(F_o^2–F_c^2)^2]/\Sigma[w(F_o^2)^2]]^{0.5}$.

Table 2
Positions and isotropic displacement parameters (Å $\times 10^3$) for Gd_4NiTe_2

Atom	*x*	*y*	*z*	U_{eq}[a]
Gd1	0.1327(1)	1/4	0.4173(1)	7(1)
Gd2	0.0417(1)	1/4	0.7016(1)	7(1)
Gd3	0.2747(1)	1/4	0.1314(1)	7(1)
Gd4	0.1034(1)	3/4	0.9656(1)	7(1)
Te1	0.0734(1)	1/4	0.1564(1)	7(1)
Te2	0.2800(1)	3/4	0.3426(2)	8(1)
Ni1	0.0473(2)	3/4	0.5282(3)	9(1)

[a] U_{eq} is defined as one-third of the trace of the orthogonalized U_{ij} tensor.

Gd_4NiTe_2 crystal. A total of 2626 reflections ($5^\circ < 2\theta \leqslant 56.5^\circ$) were collected, of which 607 were unique ($R_{int} = 0.1799$). A total of 32 variables were used in the refinements and data converged to $R_1 = 0.0661$, w$R_2 = 0.1574$ (all data). Similarly, the X-ray single-crystal structure of $Er_5Co_2Te_2$ was also determined. A hemisphere of data was collected ($5^\circ < 2\theta \leqslant 56.5^\circ$). Of 6626 reflections collected, 1215 were unique ($R_{int} = 0.1703$). A total of 32 variables were used in the refinements and data converged to $R_1 = 0.0979$, w$R_2 = 0.1202$ (all data). Crystallographic data for Gd_4NiTe_2, $Er_5Ni_2Te_2$, and $Er_5Co_2Te_2$ are summarized in Table 1. The atomic positions and isotropic displacement factors are given in Tables 2 and 3.

Routine X-ray powder diffraction data were collected using Cu$K\alpha_1$ ($\lambda = 1.5406$ Å) radiation on a Philips X-ray Generator with a mounted Guinier Camera with germanium monochromator or using the GADDS (General Area Detector Diffraction System) V4.1.08 by Bruker AXS.

Table 3
Positions and equivalent isotropic displacement parameters (Å $\times 10^3$) for $Er_5M_2Te_2$ (M = Ni, Co)[a]

M	Ni			Co		
Atom	*y*	*z*	U_{eq}[b]	*y*	*Z*	U_{eq}[b]
Er1	0.0388(1)	0.6232(1)	13(1)	0.0365(1)	0.6233(1)	7(1)
Er2	0.2580(1)	0.3726(1)	13(1)	0.2567(1)	0.3713(1)	7(1)
Er3	0.6070(1)	1/4	13(1)	0.6069(1)	1/4	7(1)
Te1	0.3844(1)	0.5388(1)	13(1)	0.3825(1)	0.5374(1)	7(1)
*M*1	0.4137(4)	1/4	16(1)	0.4118(3)	1/4	7(1)
*M*2	0.8130 (4)	1/4	16(1)	0.8195(3)	1/4	7(1)

[a] $x = 0$ for all atoms.
[b] U_{eq} equals one-third of the trace of the orthogonalized U_{ij} tensor.

3. Results and discussion

3.1. Syntheses

Synthetic routes to these compounds are similar to those used to make Gd_6NiTe_2 [6]. The use of the binary rare earth late transition metal compounds Gd_3M (M = Co, Ni) apparently facilitates incorporation of the ternary element, M, in the product; elemental starting materials results in formation of GdTe as the major phase. One advantage conferred by use of the binary Gd_3M compounds (vs. elemental starting materials) is their brittleness, which allows them to be crushed into small particles that provide a larger surface area for reaction. In addition, since the reactions were run at small scales (less than 500 mg in total), use of Gd_3Ni as the nickel source reduces its relative weighing error. In contrast, rare earth metals are available as malleable chips or shavings, and therefore have a lower surface area. If metals *do* yield the desired products, they have an advantage over powders, since the latter are highly susceptible to reaction with oxygen and hydrogen. Arc melting of reactants for Gd_4NiTe_2 was not necessary for a complete reaction.

3.2. Structure and bonding

Gd_4NiTe_2 adopts a new structure type, shown in Fig. 1 in a view down its *b*-axis; important Gd–Te bond distances are listed in Table 4, intermetallic distances are in Table 5. All atoms lie on mirror planes at $y = \frac{1}{4}$ and $\frac{3}{4}$. This view of the structure highlights the Ni-centered chains in a polyhedral representation. The shortest distance between separate Gd_6Ni_2 chains, d(Gd1−Gd2) = 4.020(3) Å (marked in Fig. 1), is presumably a weak interaction. Fig. 2 illustrates structural details within the Gd_6Ni_3 tricapped trigonal prisms that form the inner cluster core of the Gd_6Ni_2 chain. The triangular faces are isosceles, with one long (4.113(2) Å = *b*) and two short (3.679(2) Å) Gd–Gd

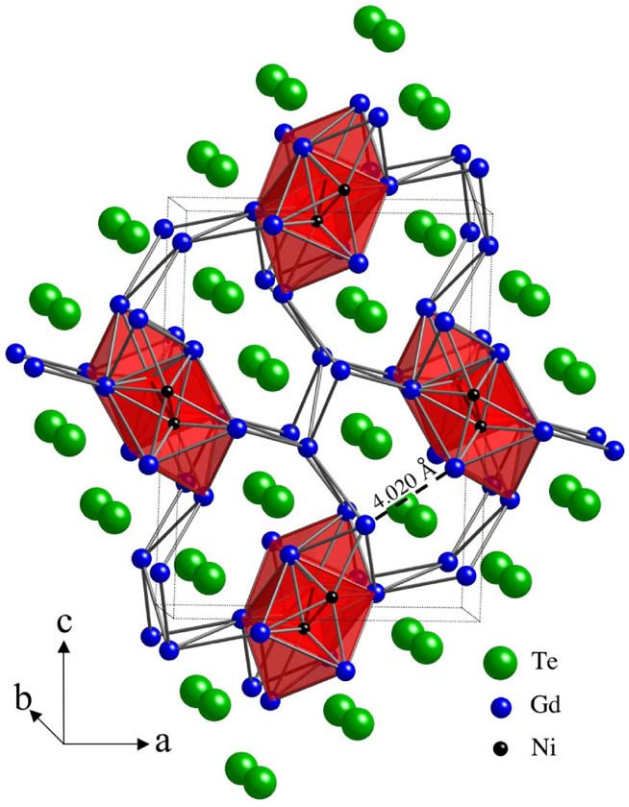

Fig. 1. Slightly off [010] projection of the Gd_4NiTe_2 structure. The Gd_6Ni_2 polyhedra are highlighted. All atoms lie on the mirror planes at $y = \frac{1}{4}$ or $\frac{3}{4}$.

Table 4
Gd–Te distances (Å) in Gd_4NiTe_2

	Distances[a]		
Gd1–Te1	3.201(3)	Gd3–Te2 (× 2)	3.225(2)
Gd1–Te2 (× 2)	3.202(2)	Gd3–Te2	3.499(3)
Gd2–Te1 (× 2)	3.196(2)	Gd4–Te1 (× 2)	3.079(2)
Gd2–Te2	3.228(2)	Gd4–Te1	3.100(2)
Gd3–Te1	3.143(3)	Gd4–Te2 (× 2)	3.099(2)

[a]All atoms also have two like neighbors at $\pm b$, 4.113(2) Å. Distance limits are 4.10 Å.

distances. Relatively short distances (d(Gd1–Gd2) = 3.614(2) Å, d(Gd1–Gd3) = 3.555(2) Å) separate the capping Gd atoms from Gd atoms making up the prism. A view of a portion of the one-dimensional condensed-cluster chain (tellurium atoms omitted) is shown in Fig. 2. The metal framework can be viewed as cluster condensation of the Ni-centered gadolinium tetrakaidecahedra along the rectangular faces of the trigonal prism so that the Ni atoms in adjacent trigonal prisms act as two of the caps to the trigonal prisms. Also recognizable is a chain of face-sharing trigonal prisms of gadolinium threaded by a zigzag chain of Ni atoms.

Table 5
Intermetallic distances, bond orders and valence electron counts for Gd_4NiTe_2

Atom	Bond	Bond distance	Pauling bond order[a]	VEC
Gd1(× 2)	−Gd1(× 2)	4.113(2)	0.035	4.057
Gd1(× 2)	−Gd2(× 2)	3.679(2)	0.188	
Gd1(× 2)	−Gd2(× 1)	3.628(2)	0.228	
Gd1(× 2)	−Gd3(× 2)	3.555(2)	0.302	
Gd1(× 2)	−Gd3(× 1)	4.020(3)	0.051	
Gd1(× 2)	−Ni1(× 2)	2.773(3)	1.016	
Gd1(× 2)	−Ni1(× 1)	2.871(4)	0.697	
Gd2(× 2)	–Gd2(× 2)	4.113(2)	0.035	2.990
Gd2(× 2)	−Gd1(× 2)	3.679(2)	0.188	
Gd2(× 2)	−Gd1(× 1)	3.628(2)	0.228	
Gd2(× 2)	−Gd3(× 2)	3.614(2)	0.241	
Gd2(× 2)	−Gd4(× 2)	3.843(2)	0.100	
Gd2(× 2)	−Ni1(× 2)	2.897(3)	0.631	
Gd2(× 2)	−Ni1(× 1)	3.035(4)	0.372	
Gd3(× 2)	−Gd3(× 2)	4.113(2)	0.035	1.766
Gd3(× 2)	−Gd1(× 2)	3.555(2)	0.302	
Gd3(× 2)	−Gd1(× 1)	4.020(3)	0.051	
Gd3(× 2)	−Gd2(× 2)	3.614(2)	0.241	
Gd3(× 2)	−Gd4(× 2)	3.888(2)	0.084	
Gd3(× 2)	−Ni1(× 1)	3.022(4)	0.391	
Gd4(× 2)	−Gd4(× 2)	4.113(2)	0.035	0.596
Gd4(× 2)	−Gd4(× 2)	3.902(3)	0.079	
Gd4(× 2)	−Gd2(× 2)	3.843(2)	0.100	
Gd4(× 2)	−Gd3(× 2)	3.888(2)	0.084	
Ni1(× 2)	−Ni1(× 2)	2.614(5)	0.313	5.380
Ni1(× 2)	−Gd1(× 2)	2.773(3)	1.016	
Ni1(× 2)	−Gd1(× 1)	2.871(4)	0.697	
Ni1(× 2)	−Gd2(× 2)	2.897(3)	0.631	
Ni1(× 2)	−Gd2(× 1)	3.035(4)	0.372	
Ni1(× 2)	−Gd3(× 1)	3.022(4)	0.391	

[a]D_1(Gd–Gd) = 3.243 Å, D_1(Gd–Ni) = 2.777 Å, D_1(Ni–Ni) = 2.311 Å; Pauling bond order n: $\log_{10} n = (D_1 - D_n)/0.6$

Pauling bond order sums are tabulated in Table 5. These have been computed with tellurium regarded as Te^{2-}, and so computed valence electron count (VEC) figures reflect only electrons devoted to Gd–Gd and Gd–Ni bonding. Single bond radii are obtained for Gd and Ni by use the Pauling bond order formula, elemental structural data [17] and respective valences of 3 and 6. A comparison of VECs among Gd atoms is consistent with our depiction of the structure: virtually all the metal–metal bonding occurs within condensed Gd_3Ni chains. The 'isolated' Gd4 atoms may be formally regarded as a Gd^{III} ions; if we sum all the VECs for all the other Gd and the Ni atoms, we obtain $28.39e^-$ per Gd_6Ni_2 unit (or $29.58e^-$ if the Gd4 contribution is considered to be donated to the chain). If the formula is written to reflect formal electron counting assignments, $Gd_4NiTe_2 \times 2 = (Gd^{3+})_2(Gd_6Ni_2^{2+})(Te^{2-})_4$, then there are 36 electrons per Gd_6Ni_2 unit available for bonding in the chain if *all* the surplus valence electrons are assigned to metal–metal bonding. However, it should be noted that the Pauling Ni

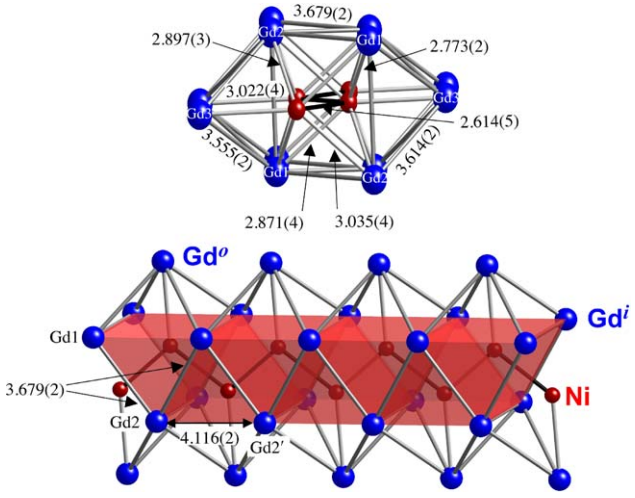

Fig. 2. Two views of the Gd_6Ni_2 chain imbedded in Gd_4NiTe_2, with numbering scheme and selected bond distances (Å) marked.

single-bond radius was originally calculated by assigning only 6 electrons to nickel (cf. p. 397, Ref. [18]). If we are consistent with this assignment, then we should perhaps expect to find only 28 electrons for the summed VEC—remarkably close to $28.39e^-$. This assignment is, of course, in closer correspondence with the individual Ni atom VEC of $5.38e^-$.

While the internal consistency of bond sums is a source of some interest, one should not attach too much physical significance to the individual atom VECs. Even if the 'missing' 4 Ni electrons are added to the computed VEC (an omission which Pauling associated with the rather contracted nature of the Ni 3*d* orbitals), the Ni 'charge' would still be positive. We view this as unlikely since the nickel atoms are bound only to more electropositive gadolinium. Similarly, if the VECs for the Gd atoms are literally equated with electron densities, Gd1 is quite anionic (−1.06), Gd2 is virtually neutral, and Gd3 would be +1.23. Clearly, a physical partitioning of the Gd–Ni bonds would reflect the highly polar nature of those bonds—as is seen in band structure calculations we have presented for similar compounds in the past [7,19–21].

A near-[100] projection of the $Er_5M_2Te_2$ (M = Co, Ni) structure is shown in Fig. 3a. Er_6M_2 chains homologous to the Gd_6Ni_2 chain already discussed interconnect by sharing the capping Er1 atoms to form layers that propagate in the *ab* plane (Fig. 3b). These Er–Er/Er–M bonded layers (normal to vertical on the page) are separated by Te atoms. A view down on one Er_5M_2 layer in Fig. 3b clearly shows the condensation of the Er_6M_2 chains at the Er1 position and $a/2$ shift in the zigzag M chains on moving between adjacent chains. The overall 3D framework is formed when layers stack up the *c*-axis with displacements of 3.170(4) Å (M = Ni) and 3.190(4) Å (M = Co) along the *b* direction between adjacent layers. This displacement (~0.214*b*) results in

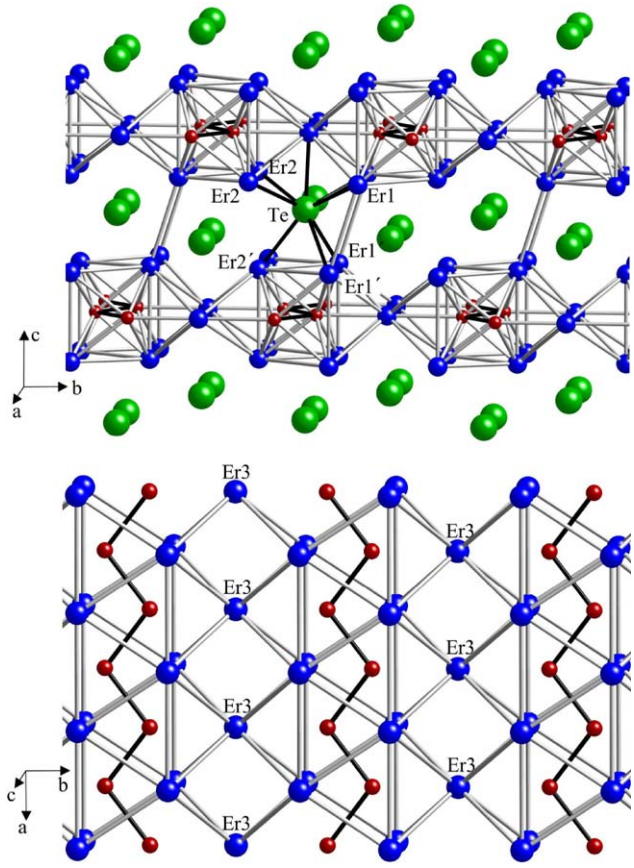

Fig. 3. (a) Near [100] projection of the $Er_5M_2Te_2$ structure showing the environment of one Te atom. (b) An Er_5M_2 layer (*ab*-plane slice) highlighting links via Er1 atoms and zig-zag M-atom chains.

efficient packing around Te atoms that occupy voids with an eight-coordinate environment between the metal–metal bonded layers. Te–Er distances range from 3.079 to 3.314 Å. As seen in many other metal-rich telluride compounds, the shortest Te–Te distance is equal to the short crystallographic axis and is close to the van der Waal's diameter of Te. Important metal–metal distances are listed in Table 6.

Isolated R_6M_2 chains like those found in Gd_4NiTe_2 are also found in a series of iodide compounds with the composition R_3MI_3; these include Gd_3MnI_3 [9], Y_3MI_3 (M = Ru, Ir), [10] and other members with R = La, Pr, Gd, Er, and Y with M = Ru and Ir. In these compounds however, there are no rare-earth atoms beyond those in the intermetallic chains. It is not clear whether telluride phases isostructural to the iodides might be synthesized, but in more rare-earth-rich tellurides condensation of the chains into layers (e.g., $Y_5Ni_2Te_2$) [11] and double chains (e.g., $Sc_5Ni_2Te_2$) [2] occurs.

Illustrations comparing the extended metal chain structures and are presented in Fig. 4. Within these compounds, there is considerable structural flexibility that distinguishes the other phases from the monoclinic R_3MI_3. Gd_4NiTe_2 is the first chalcogenide compound to

Table 6
Important metal–metal distances (Å) for $Er_5M_2Te_2$ (M = Co, Ni)

Bonds	M = Co	M = Ni
Er3–Er2 (× 5)	3.472(1)	3.482(2)
Er1–Er3 (× 5)	3.455(1)	3.466(2)
Er2–Er2 (× 1)	3.614(2)	3.606(3)
Er3–Er3 (× 1)	3.8976(8)	3.934(1)
Er1–Er3 (× 4)	3.650(1)	3.596(2)
Er1–Er1 (× 1)	3.774(2)	3.732(3)
M2–Er1 (× 1)	2.911(5)	3.051(7)
M2–Er2 (× 3)	2.936(4)	2.790(2)
M2–Er3 (× 5)	2.820(2)	2.881(5)
M1–Er3 (× 1)	3.172(5)	2.864(7)
M1–Er2 (× 3)	2.818(2)	2.926(5)
M1–Er1 (× 5)	2.859(4)	2.801(2)
M1–M2 (× 4)	2.386(4)	2.468(6)

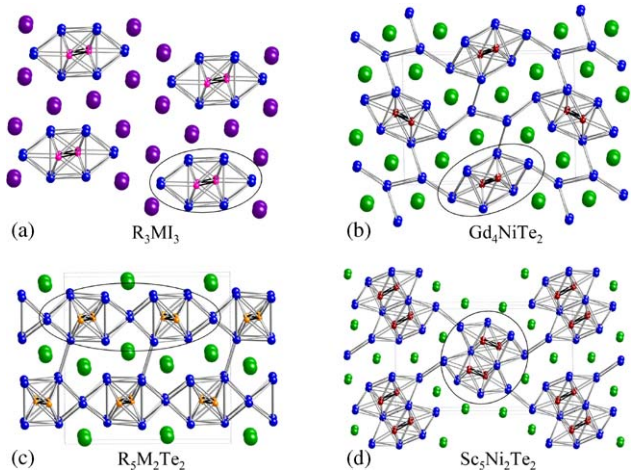

Fig. 4. Structural relationship between (a) Gd_4NiTe_2, (b) $R_5M_2Te_2$ (R = Er, Y; M = Fe, Ni, Co), and (c) $Sc_5Ni_2Te_2$ illustrating the alternative condensation modes of the of the single 1-D chain in Gd_4NiTe_2.

incorporate the R_6M_2 double chain. The Mn-centered double chain units found in Gd_3MnI_3 are much less symmetrical than the Gd_6Ni_2 chain in Gd_4NiTe_2. In $Sc_5Ni_2Te_2$ (Fig. 4d), condensation occurs at just the rare-earth-atom positions that are *not* shared in $Er_5M_2Te_2$ (Fig. 4c). Double chains of Ni-centered units that share trans edges and are further condensed side-by-side occur in $Sc_5Ni_2Te_2$; vertex condensation to form layers in the $R_5M_2Te_2$ (R = Y, Er; M = Fe, Co, Ni) structure.

Comparison of Gd_4NiTe_2 and the structurally related Ni-containing compounds $Sc_5Ni_2Te_2$ and $Er_5Ni_2Te_2$ reveals some interesting contrasts in these Ni-centered chains (Table 7). Ni–Ni distances and some VECs are given in Table 6. The Ni–Ni distance (2.468(6) Å) in $Er_5Ni_2Te_2$ is markedly shorter than the corresponding distances in Gd_4NiTe_2 (2.614(6) Å) and $Sc_5Ni_2Te_2$ (2.657(2) Å). The nickel VECs are considerably larger

Table 7
Comparison of M–M and bond lengths and Pauling bond orders for Gd_4NiTe_2, $Sc_5Ni_2Te_2$, and $Er_5Ni_2Te_2$

Compound	Bonds	d(Ni–Ni)/d(R–Ni) (Å)	Bond order[a]
Gd_4NiTe_2	Ni1–Ni1(× 2)	2.614(5)	0.313
	Ni1–Gd1(× 2)	2.773(3)	1.016
	Ni1–Gd1(× 1)	2.871(4)	0.697
	Ni1–Gd2(× 2)	2.897(3)	0.631
	Ni1–Gd2(× 1)	3.035(4)	0.372
	Ni1–Gd3(× 1)	3.022(4)	0.391
$Er_5Ni_2Te_2$	Ni1–Ni2(× 4)	2.468(6)	0.547
	Ni1–Er1(× 1)	3.051(7)	0.293
	Ni1–Er2(× 3)	2.790(2)	0.800
	Ni1–Er3(× 3)	2.881(5)	0.565
	Ni2–Er1(× 1)	2.864(7)	0.603
	Ni2–Er2(× 3)	2.926(5)	0.475
	Ni2–Er3(× 3)	2.801(2)	0.767
$Sc_5Ni_2Te_2$	Ni1–Ni2(× 2)	2.657(2)	0.265
	Ni1–Sc1(× 2)	2.624(2)	0.970
	Ni1–Sc2(× 1)	2.699(4)	0.727
	Ni1–Sc4(× 2)	2.635(3)	0.930
	Ni1–Sc4(× 1)	2.864(4)	0.386
	Ni1–Sc5(× 1)	2.653(4)	0.868
	Ni2–Sc1(× 1)	2.874(4)	0.372
	Ni2–Sc3(× 1)	2.665(4)	0.829
	Ni2–Sc4(× 2)	2.622(3)	0.977
	Ni2–Sc4(× 1)	2.862(4)	0.389
	Ni2–Sc5(× 2)	2.608(2)	1.031

[a] D_1(Ni–Ni) = 2.311 Å, D_1(Ni–Gd) = 2.777 Å, D_1(Sc–Ni) = 2.616 Å, D_1(Er–Ni) = 2.732 Å.

for the scandium compound than for the two lanthanide-containing compounds. The origins of these differences are not readily apparent; explanations may become clearer as synthetic exploration yield more data from which trends can be extracted.

4. Conclusions

The new compounds, Gd_4NiTe_2 and $Er_5M_2Te_2$ (M = Ni, Co), were synthesized by high-temperature solid-state reactions and crystallize in the orthorhombic *Pnma* and *Cmcm* space groups, respectively. Gd_4NiTe_2 is the first chalcogenide to exhibit infinite Gd_6Ni_2 double-chains, a motif long known for lanthanide-iodides with the R_3MI_3 structure-type. The $Er_5M_2Te_2$ compounds are isostructural to the lighter rare earth homolog, $Y_5Ni_2Te_2$. The prevalence of tricapped trigonal prisms throughout these compounds' structures demonstrate their electronic and structural flexibility. These compounds further extend the number of chalcogenide examples wherein early late transition metal bonding in to electron poorer rare-earth metals is of prime importance. With increasing late transition metal contents, there is a progression of TTP units to link together to form single chains, then double chains, then layers and 3-D networks. This is illustrated by the

structural comparison between $R_5M_2Te_2$ ($R = Y$, Er; $M = Co$, Ni) and $Sc_5Ni_2Te_2$. Synthetic efforts in this area continue and discovery leads to new materials whose compositions and structure show ever more versatility.

Acknowledgments

We thank the Robert A. Welch Foundation for its support through Grant A-1132 and the Texas Advanced Research Program through Grant # 010366-0188-200.

References

[1] L. Brewer, P.R. Wengert, Metall. Trans. 4 (1973) 2674.
[2] P.A. Maggard, J.D. Corbett, Inorg. Chem. 38 (1999) 1945–1950.
[3] N. Bestaoui, P.S. Herle, J.D. Corbett, J. Solid State Chem. 155 (2000) 9–14.
[4] P.A. Maggard, J.D. Corbett, Inorg. Chem. 39 (2000) 4143–4146.
[5] C. Wang, T. Hughbanks, Inorg. Chem. 35 (1996) 6987–6994.
[6] F. Meng, C. Magliocchi, T. Hughbanks, J. Alloys Compd. 358 (2003) 98–103.
[7] R.L. Abdon, T. Hughbanks, J. Am. Chem. Soc. 117 (1995) 10035–10040.
[8] F. Meng, T. Hughbanks, Inorg. Chem. 40 (2001) 2482–2483.
[9] M. Ebihara, J.D. Martin, J.D. Corbett, Inorg. Chem. 33 (1994) 2079–2084.
[10] M.W. Payne, P.K. Dorhout, S.-J. Kim, T.R. Hughbanks, J.D. Corbett, Inorg. Chem. 31 (1992) 1389.
[11] P.A. Maggard, J.D. Corbett, J. Am. Chem. Soc. 122 (2000) 10740–10741.
[12] K.A.J. Gschneider, J. Mater. Eng. Performance 7 (1998) 656–660.
[13] SMART, Software for the CCD Detector System, Bruker Analytical X-ray System: Madison, WI, 1995.
[14] SAINTPLUS, Software for the CCD Detector System, Madison, WI, 1999.
[15] G.M. Sheldrick, SADABS: Program for Absorption Corrections, Institute für Anorganishe Chemie der Universität Göttingen, Göttingen, Germany, 1999.
[16] G.M. Sheldrick, SHELXTL-PLUS an Integrated System for Solving Refining and Displaying Crystal Structures from Diffraction Data, Nicolet Analytical X-ray Instruments, Göttingen, Germany, 1988.
[17] J. Donohue, The Structures of the Elements, Krieger, New York, 1982.
[18] L. Pauling, The Nature of the Chemical Bond, third ed., Cornell University Press, Ithaca, New York, 1960.
[19] T. Hughbanks, in: T.P. Fehlner (Ed.), Inorganometallic Chemistry. Plenum Press,, New York, 1992, pp. 289–331 (Section).
[20] K.A. Yee, T. Hughbanks, Inorg. Chem. 30 (1991) 2321.
[21] K.S. Nanjundaswamy, T. Hughbanks, J. Solid State Chem. 98 (1992) 278.